OPEN ACCESS
JOURNAL OF ADVANCED DIELECTRICS
Vol. 13, No. 2 (2023) 2350006 (11 pages)

DOI: 10.1142/S2010135X23500066

Large piezoelectric anisotropy and high hydrostatic piezoelectric activity due to an appreciable orientation effect and porosity in novel 2–2–0 composites*

Vitaly Yu. Topolov[†,§] Andrey V. Krivoruchko[‡] and Natalia V. Prutsakova[‡]
[†]*Department of Physics, Southern Federal University, 5 Zorge Street*
Rostov-on-Don 344090, Russia
[‡]*Don State Technical University, 1 Gagarin Square*
Rostov-on-Don 344000, Russia
[§]vutopolov@sfedu.ru

Received 1 December 2022; Revised 26 January 2023; Accepted 13 February 2023; Published 27 March 2023

The polarization orientation effect and porosity effect on the piezoelectric properties and related parameters are studied in 2–2-type composites based on domain-engineered relaxor-ferroelectric [011]-poled single crystals. The parameters, which are of great interest, are an anisotropy of the piezoelectric coefficients d_{3j}^*, an anisotropy of the energy-harvesting figures of merit $d_{3j}^* g_{3j}^*$ and the hydrostatic piezoelectric coefficient d_h^*. An orientation of the main crystallographic axes in each polydomain single-crystal layer is described by angles β and γ. Diagrams built for the first time show the (β, γ) regions, where a large anisotropy of d_{3j}^* (or $d_{3j}^* g_{3j}^*$) is achieved, and where inequality $d_h^* > 1000$ pC/N holds. A large local max $d_h^* = 1930$ pC/N is achieved in a 2–2–0 PZN–0.065PT-based composite at the longitudinal piezoelectric coefficient $d_{33}^* = 2290$ pC/N and figure of merit $d_{33}^* g_{33}^* = 1.02 \cdot 10^{-9}$ Pa^{-1}. The aforementioned large parameters are to be of value in piezoelectric sensing, energy harvesting and hydroacoustics.

Keywords: Piezo-active composite; 2–2-type; orientation effect; porosity; large piezoelectric anisotropy.

1. Introduction

Advanced composite materials based on relaxor-ferroelectric single crystals (SCs) with specific non180° domain structures obtained on poling in an electric field show a high piezoelectric performance[1–5] that is of importance in sensor, hydroacoustic, energy-harvesting, medical-device and other important applications.[6–11] The typical SC components[1,3,4,5,7–9,11] are domain-engineered samples from two-component relaxor-ferroelectric solid solutions such as $(1 - x)Pb(Mg_{1/3}Nb_{2/3})O_3 - xPbTiO_3$ (PMN–xPT) and $(1 - y)Pb(Zn_{1/3}Nb_{2/3})O_3 - yPbTiO_3$ (PZN–yPT). The PMN–xPT and PZN–yPT compositions with the perovskite-type structure are chosen near the morphotropic phase boundary for achieving a high piezoelectric activity and strong electromechanical coupling in SCs.[6] For instance, the large longitudinal piezoelectric coefficient $d_{33} \sim 10^{-9}$ C/N and electromechanical coupling factor $k_{33} \approx 0.9$ of the domain-engineered PMN–xPT and PZN–yPT SCs[6] poled along specific crystallographic directions are larger than the d_{33} and k_{33} values of conventional ferroelectric perovskite-type ceramics[7,8] and are advantageous for actuator and transducer applications. In some composites, three-component relaxor-based solid solutions are used[2,10] to form the SC component and achieve large effective piezoelectric coefficients and other parameters for specific applications. A great potential of the piezo-active SC-based composites is concerned with (i) an optimum orientation of the main crystallographic axes of SC and its spontaneous polarization vector, and (ii) specifics of the composite microgeometry. These factors, along with the properties of components,[7,8] are to be taken into account when manufacturing piezo-active composites.

The PMN–xPT and PZN–yPT SCs suitable for applications are poled along specific perovskite unit-cell directions,[1,6] e.g., [001], [011] or [111], and this poling leads to engineered domain structures or single-domain states. A full set of electromechanical (i.e., elastic, piezoelectric and dielectric) constants[13–15] of the poled SC is found by means of experimental methods. The PMN–xPT and PZN–yPT SCs become the main piezoelectric components of laminar composites[1–3,6–8,12] that are characterized by 2–2 and related connectivity patterns in terms of work.[7,8,16] Applications of the 2–2-type composites[1–3] strongly depend on their effective piezoelectric properties, electromechanical coupling, hydrostatic, energy-harvesting parameters,[7,8,12] etc. Specifics of the piezoelectric effect and related energy-harvesting figures of merit were recently studied[12] in 2–2-type composites

*This paper was originally submitted to the Special Issue on Piezoelectric Materials and Devices published in December 2022.

§Corresponding author.

based on the domain-engineered [011]-poled PZN–*y*PT SCs. A simple rotation of the main crystallographic axes *X* and *Y* around *Z* (i.e., around the poling axis of SC) was taken into account[12] in the SC layers poled along [011]. However, till date, the performance of 2–2-type composites based on the [011]-poled SCs is yet to be described in the literature for a case of rotations of the main crystallographic axes of the SC component around two co-ordinate axes, and no comparison of the parameters of the PZN–*y*PT- and PMN–*x*PT-based composites at such rotations was made. Moreover, the effect of porosity of the non-crystalline layers on the effective properties has yet to be discussed in detail for 2–2-type composites wherein the [011]-poled SCs are the main piezoelectric components. The aim of the present paper is (i) to analyze the role of the polarization orientation effect and porosity effect, which act together in the 2–2-type composite based on the [011]-poled SC, and (ii) to compare the effective parameters of the similar 2–2-type PMN–*x*PT- and PZN–*y*PT-based composites, where molar concentrations *x* and *y* are taken from regions near the morphotropic phase boundary.

2. Modeling

2.1. *Model concepts*

In the 2–2-type composite to be considered, there are layers of two types (Fig. 1(a)), and these layers are parallel-connected and arranged regularly along the OX_1 axis of the rectangular co-ordinate system ($X_1X_2X_3$). The layers are continuous along the OX_2 and OX_3 axes. The Type I layer is the domain-engineered SC poled along [011] of the perovskite unit cell, and the volume fraction of Type I layers in the composite sample equals *m*. The $\boldsymbol{P}_{s,1}$ and $\boldsymbol{P}_{s,2}$ vectors characterize the spontaneous polarization of the non180° domains in the Type I layer, and its spontaneous polarization is characterized by the $\boldsymbol{P}_s^{(1)}$ vector (see inset 1 of Fig. 1(a)). Main crystallographic axes *X*, *Y* and *Z* in the Type I layer are arranged as shown in inset 1 of Fig. 1(a).

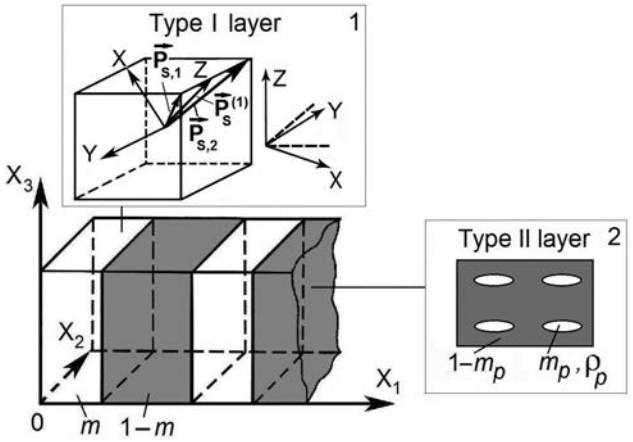

(a)

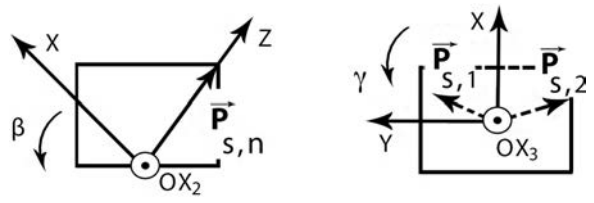

(b)

Fig. 1. (a) Schematic of the 2–2–0 composite based on the [011]-poled SC and (b) modes of the rotation of the main crystallographic axes *X*, *Y* and *Z* in the SC component.

The Type II layer is a porous polymer with 3–0 connectivity (see inset 2 in Fig. 1(a)). The volume fraction of the Type II layers in the composite equals $1 - m$. Each air pore in the Type II layer is assumed to be spheroidal, and the equation

$$(x_1/a_{1,p})^2 + (x_2/a_{2,p})^2 + (x_3/a_{3,p})^2 = 1 \quad (1)$$

describes the pore shape in the ($X_1X_2X_3$) system. In Eq. (1), $a_{1,p}$, $a_{2,p} = a_{1,p}$ and $a_{3,p}$ are semi-axes of the pore. The aspect ratio $\rho_p = a_{1,p} / a_{3,p}$ and volume fraction m_p of pores in each Type II layer are two parameters to be considered in describing the porosity effect in the studied composite. Centers of symmetry of these pores due to their regular arrangement form a simple tetragonal lattice. Its unit-cell vectors are assumed to be parallel to the OX_f axes shown in Fig. 1(a). Taking into account the closed pores in the Type II layers and concepts,[7,16] we describe the laminar composite shown in Fig. 1(a) by 2–2–0 connectivity.

Orientations of the main crystallographic axes *X*, *Y* and *Z* in each Type I layer are described by the matrix

$$\|r\| = \begin{pmatrix} \cos\gamma & \sin\gamma & 0 \\ -\sin\gamma & \cos\gamma & 0 \\ 0 & 0 & 1 \end{pmatrix} \begin{pmatrix} \cos\beta & 0 & \sin\beta \\ 0 & 1 & 0 \\ -\sin\beta & 0 & \cos\beta \end{pmatrix}. \quad (2)$$

In Eq. (2), β and γ are rotation angles of the main crystallographic axes in the SC component as shown in Fig. 1(b). In our opinion, this rotation mode enables one to achieve a relatively strong longitudinal piezoelectric effect in the composite due to specifics of the electromechanical properties of the [011]-poled SC component. In the initial position, at $\beta = \gamma = 0°$, the main crystallographic axes *X*, *Y* and *Z* in the Type I layer are oriented as follows: $X \parallel OX_1$, $Y \parallel OX_2$ and $Z \parallel \boldsymbol{P}_s^{(1)} \parallel OX_3$. These orientations can be also written as $X \parallel [0\bar{1}1]$, $Y \parallel [1\ 0\ 0]$ and $Z \parallel [0\ 1\ 1]$, where [*h k l*] denote directions in the perovskite unit-cell. Using the $\| r \|$ matrix from Eq. (2), one can represent the electromechanical properties of the Type I layer in the ($X_1X_2X_3$) system as tensor components

$$\begin{aligned} &\varepsilon_{mn}^{\sigma\,\prime} = r_{mp}r_{nq}\varepsilon_{pq}^{\sigma},\ d_{efg}{}' = r_{ej}r_{fk}r_{gl}d_{jkl} \text{ and} \\ &s_{rtuv}^{E\,\prime} = r_{ra}r_{tb}r_{uc}r_{vd}s_{abcd}^{E}. \end{aligned} \quad (3)$$

In Eq. (3), $\varepsilon_{pq}^{\sigma}$, d_{jkl} and s_{abcd}^{E} are components of dielectric permittivities (that form a second-rank tensor) at mechanical stress σ = const, piezoelectric coefficients (that form a

third-rank tensor) and elastic compliances (that form a fourth-rank tensor) at electric field E = const, respectively. Hereafter, we use the matrix (or two-index) form[17] to denote the aforementioned and other tensor components. Electromechanical properties from Eq. (3) can be rewritten as functions

$$\begin{aligned} &\varepsilon_{mn}^{\sigma}{}' = \varepsilon_{mn}^{\sigma}{}'(\beta,\gamma), d_{ij}{}' = d_{ij}{}'(\beta,\gamma) \quad \text{and} \\ &s_{ab}{}^{E'} = s_{ab}{}^{E'}(\beta,\gamma). \end{aligned} \tag{4}$$

Effective properties of the Type II layer (see inset 2 of Fig. 1(a)) can be found in accordance with the dilute approach:[18]

$$\| K^{(3-0)} \| = \| K^{(\mathrm{pol})} \| [\| I \| - m_p(\| I \| - (1 - m_p)\| S \|)^{-1}]. \tag{5}$$

In Eq. (5), m_p is the volume fraction of the spheroidal pores in the Type II layer, $\| K^{(\mathrm{pol})} \|$ is the 9×9 matrix of properties of monolithic polymer, $\| I \|$ is the 9×9 identity matrix and $\| S \|$ is the 9×9 matrix of components of the electroelastic Eshelby tensor[19] that depends on the aspect ratio ρ_p of the pore and on the properties of monolithic polymer (either isotropic or transversely isotropic). The properties of the monolithic polymer component are characterized by the matrix written in the general form as follows:

$$\left\| K^{(pol)} \right\| = \begin{pmatrix} \left\| c^{(\mathrm{pol}),E} \right\| & \left\| e^{(\mathrm{pol})} \right\|^t \\ \left\| e^{(\mathrm{pol})} \right\| & -\left\| \varepsilon^{(\mathrm{pol}),\xi} \right\| \end{pmatrix}. \tag{6}$$

In Eq. (6), $\| c^{(\mathrm{pol}),E} \|$ is the 6×6 matrix of elastic moduli at E = const, $\| e^{(\mathrm{pol})} \|$ is the 3×6 matrix of piezoelectric coefficients, and $\| \varepsilon^{(\mathrm{pol}),\xi} \|$ is the 3×3 matrix of dielectric permittivities at mechanical strain ξ = const. Superscript t is used in Eq. (6) to denote the matrix transposition. Structures of the $\| K^{(3-0)} \|$ matrix from Eq. (5) and the $\| K^{(\mathrm{pol})} \|$ matrix from Eq. (6) are similar. We find the $\| K^{(3-0)} \|$ matrix elements and, therefore, the effective properties of porous polymer in accordance with the so-called long-wave approximation.[7,8] This approximation means that the longest semi-axis of the spheroidal pore in the Type II layer (see inset 2 in Fig. 1(a)) is much smaller than the thickness of any layer of the studied composite.

2.2. *Effective properties and related parameters*

The effective electromechanical properties of the composite shown in Fig. 1(a) are found by using the matrix method.[7,8] The main formula that describes the effective properties is written as follows:

$$\begin{aligned} \| C^* \| = [\| C^{(1)} \| \cdot \| M \| m + \| C^{(2)} \| (1 - m)] \\ [\| M \| m + \| I \| (1 - m)]^{-1}. \end{aligned} \tag{7}$$

In Eq. (7),

$$\left\| C^{(n)} \right\| = \begin{pmatrix} \left\| s^{(n),E} \right\| \left\| d^{(n)} \right\|^t \\ \left\| d^{(n)} \right\| \quad \left\| \varepsilon^{(n),\sigma} \right\| \end{pmatrix}, \tag{8}$$

where n = 1 and 2. The $\| C^{(n)} \|$ matrix from Eq. (8) is the 9×9 matrix of the properties of Type I (n = 1) or Type II (n = 2) layer. In Eq. (7), m is the volume fraction of the Type I layers, $\| M \|$ is the 9×9 matrix associated with the boundary conditions[7,12] for mechanical and electric fields at interfaces x_1 = const in the composite sample (see Fig. 1(a)), and $\| I \|$ is the 9×9 identity matrix. In Eq. (8), $\| s^{(n),E} \|$ is the 6×6 matrix of elastic compliances at E = const, $\| d^{(n)} \|$ is the 3×6 matrix of piezoelectric coefficients, and $\| \varepsilon^{(n),\sigma} \|$ is the 3×3 matrix of dielectric permittivities at σ = const. The $\| C^{(1)} \|$ matrix characterizes the electromechanical properties in accordance with the rotation modes in Fig. 1(b) and Eqs. (2)–(4). The $\| C^{(2)} \|$ matrix from Eq. (7) is found by using the $\| K^{(3-0)} \|$ elements from Eq. (5) and formulae[17] for electromechanical properties of a piezoelectric medium. The $\| C^{(2)} \|$ elements depend on the aspect ratio ρ_p and volume fraction m_p of pores in the Type II layer. The $\| C^* \|$ elements from Eq. (7) are functions of m, β, γ, ρ_p and m_p. By analogy with the properties of the Type II layer, the effective properties expressed by Eq. (7) are determined in the long-wave approximation.[7,8] According to this approximation, any wavelength of an external field is much longer than the thickness of an individual layer of the composite sample.

Based on the $\| C^* \|$ matrix elements from Eq. (7), we evaluate the following effective parameters of the 2–2–0 composite:

(i) Piezoelectric coefficients d_{3j}^* and related anisotropy factors

$$\zeta_{d1}^* = d_{33}^* / d_{31}^* \text{ and } \zeta_{d2}^* = d_{33}^* / d_{32}^*, \tag{9}$$

(ii) Hydrostatic (or hydrophone) piezoelectric coefficient

$$d_h^* = d_{33}^* + d_{32}^* + d_{31}^*. \tag{10}$$

(iii) Traditional (or squared)[7] energy-harvesting figures of merit

$$(Q_{3j}^*)^2 = d_{3j}^* g_{3j}^*, \tag{11}$$

where j = 1, 2 and 3. The piezoelectric coefficient g_{3j}^* from Eq. (11) is to be found from the formula[17]

$$d_{3j}^* = g_{3j}^* \varepsilon_{jj}^{*\sigma}. \tag{12}$$

Equation (10) is written on assumption that electrodes applied to the sample are parallel to the (X_1OX_2) plane, see Fig. 1(a). The piezoelectric coefficient d_h^* from Eq. (10) is used to describe the piezoelectric activity of the composite under hydrostatic loading. Energy-harvesting figures of merit $(Q_{3j}^*)^2$ from Eq. (11) are introduced to evaluate the signal-to-noise ratio of the composite[7] that acts as a piezoelectric sensor. By analogy with the effective properties of the composite [see Eq. (7)], we analyze the effective parameters from Eqs. (9)–(12) as functions of the volume fraction m, rotation angles β and γ (Type I layer), and aspect ratio ρ_p and porosity m_p (Type II layer).

Table 1. Elastic compliances s^E_{ab} (in 10^{-12} Pa^{-1}), piezoelectric coefficients d_{ij} (in pC/N) and dielectric permittivities ε^σ_{pp} of domain-engineered [011]-poled SCs (*mm*2 symmetry) and isotropic polymer at room temperature.

	PZN–0.065PT SC, Ref. 15	PMN–0.29PT SC, Ref. 14	Polyurethane, Ref. 7
s^E_{11}	46.99	18.0	405
s^E_{12}	–74.01	–31.1	–151
s^E_{13}	39.51	8.4	–151
s^E_{22}	170.69	11.2	405
s^E_{23}	–96.76	–61.9	–151
s^E_{33}	61.47	49.6	405
s^E_{44}	15.04	14.9	1112
s^E_{55}	333.33	69.4	1112
s^E_{66}	169.08	13.0	1112
d_{15}	4871	1188	0
d_{24}	121	167	0
d_{31}	1191	610	0
d_{32}	–2618	–1883	0
d_{33}	1571	1030	0
$\varepsilon^\sigma_{11}/\varepsilon_0$	9500	3564	3.5
$\varepsilon^\sigma_{22}/\varepsilon_0$	1500	1127	3.5
$\varepsilon^\sigma_{33}/\varepsilon_0$	5600	4033	3.5

Our evaluations of the piezoelectric performance and effective parameters from Eqs. (9)–(12) were carried out by using the full sets of experimental electromechanical constants of the [011]-poled domain-engineered SC and monolithic polymer components (Table 1). The [011]-poled PMN–0.29PT and PZN–0.065PT SCs with domain types shown in inset 1 of Fig. 1(a) are from the *mm*2 symmetry class.[14,15] We note that the PMN–0.29PT and PZN–0.065PT compositions are located a few percent away from the morphotropic phase boundary,[20] in the region of the stable ferroelectric rhombohedral 3*m* phase. In contrast to the aforementioned SCs, polyurethane is considered as a piezo-passive polymer[7,8] in the Type II layer.

3. Results and Discussion

3.1. *Large anisotropy of d^*_{3j} and $(Q^*_{3j})^2$, and new $\beta-\gamma$ diagrams*

Taking the properties and symmetry of components (see Table 1) as well as the porous structure in the Type II layer (see inset 2 in Fig. 1(a)) into account, we analyze the orientation dependence of the effective electromechanical properties [see Eq. (7)] and hydrostatic piezoelectric coefficient d^*_h of the 2–2–0 composite [see Eq. (10)]. Our results show the validity of the condition

$$d^*_h(m, \beta, \gamma, m_p, \rho_p) = d^*_h(m, 90^\circ + \beta, 180^\circ - \gamma, m_p, \rho_p). \quad (13)$$

In Eq. (13), d^*_h is the hydrostatic piezoelectric coefficient from Eq. (10). Considering Eq. (13), we vary the rotation angles β and γ in Type I layers from 0° to 90°. The aspect ratio ρ_p of the pore in the Type II layer is varied from 0.1 (the heavily prolate pore) to 100 (the heavily oblate pore).

Important information on a large piezoelectric anisotropy is concentrated in the $\beta-\gamma$ diagrams (Figs. 2 and 3) built for

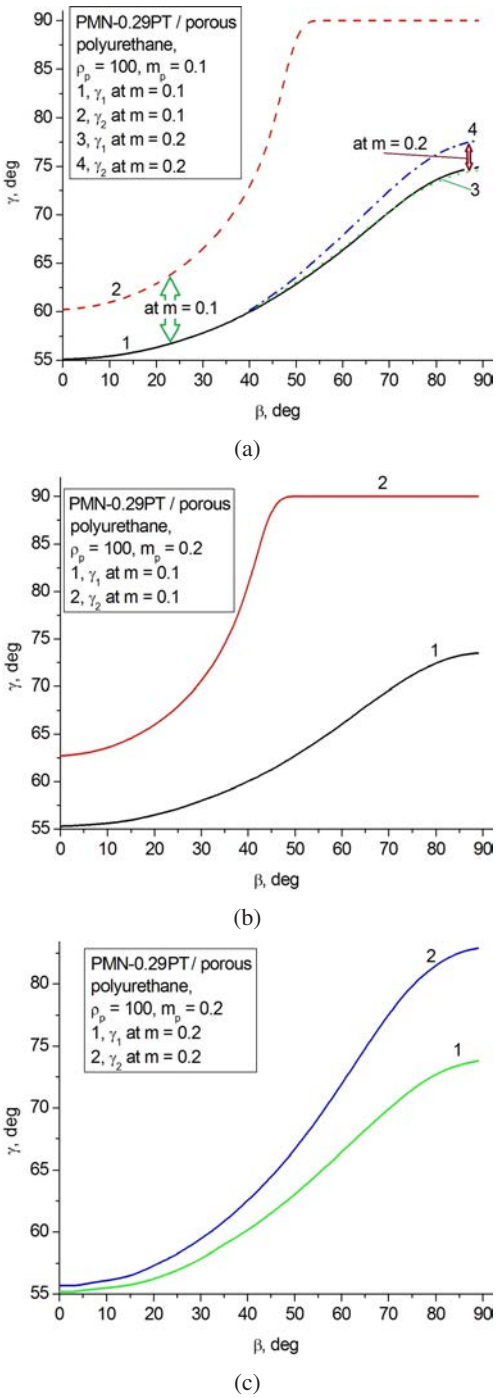

Fig. 2. $\beta-\gamma$ diagrams of regions of the large anisotropy of piezoelectric coefficients d^*_3 in the 2–2–0 PMN–0.29PT SC/porous polyurethane composite. In the range of $[\gamma_1; \gamma_2]$, conditions (14) hold.

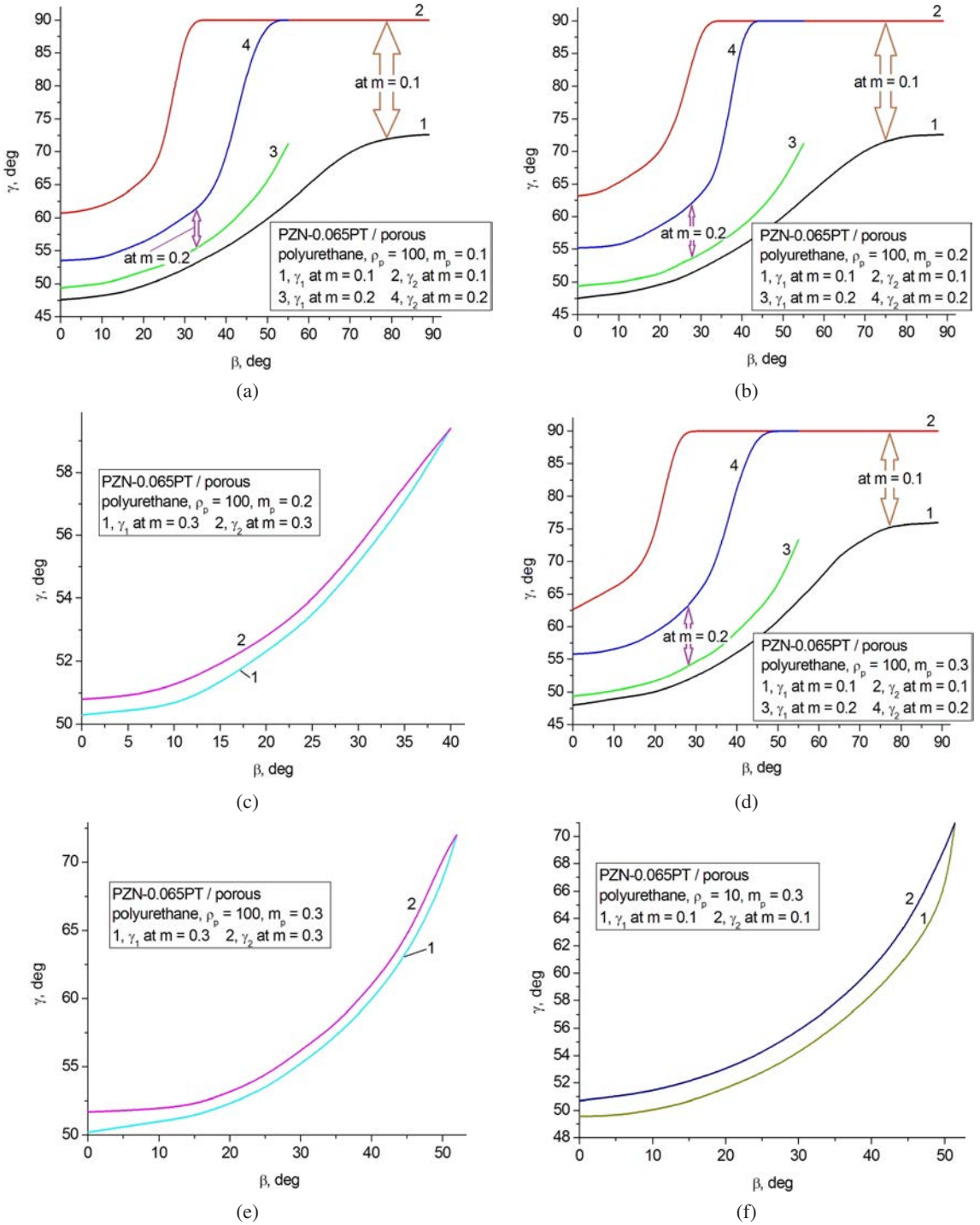

Fig. 3. β–γ diagrams of regions of the large anisotropy of piezoelectric coefficients d_3^{j*} in the 2–2–0 PZN–0.065PT SC/porous polyurethane composite. In the range of $[\gamma_1; \gamma_2]$, conditions (14) hold.

the first time. Two conditions for the large anisotropy of d_{3j}^* of the composite are written as follows:

$$| \zeta_{d1}{}^* | \geq 5 \text{ and } | \zeta_{d2}{}^* | \geq 5. \quad (14)$$

We note that condition (14) hold in the $[\gamma_1;\gamma_2]$ range, and the difference $\gamma_2 - \gamma_1$ depends on the β angle (see Figs. 2 and 3). The volume fraction m, aspect ratio ρ_p and porosity m_p are regarded as parameters in each diagram from Figs. 2 and 3. It should be noted that the heavily oblate shape of the pore ($\rho_p >> 1$) is preferable to provide a large piezoelectric coefficient $d_{33}{}^*$ of the composite and to weaken a transversal piezoelectric response concerned with $d_{31}{}^*$ and $d_{32}{}^*$. Such an

effect of the porous medium is mainly achieved due to the large ratio of elastic compliances $s_{33}^{(3-0)}$ / $s_{11}^{(3-0)}$ in the Type II layer at $\rho_p >> 1$. We emphasize that in the wide β and γ ranges, the longitudinal piezoelectric coefficient d_{33}^* of the PMN–0.29PT- and PZN–0.065PT-based composites is positive and makes a prevalent contribution in the hydrostatic piezoelectric coefficient d_h^* from Eq. (10).

Graphs in Figs. 2 and 3 suggest that the Type II layers with the heavily oblate pores at the aspect ratio $\rho_p = 100$ play the key role in forming the large piezoelectric anisotropy in both the studied 2–2–0 composites. However, conditions (14) hold in a narrower range of porosity m_p in the Type II layers of the PMN–0.29PT-based composite. At $\rho_p = 10$–100 and $m_p = 0.3$, conditions (14) are valid for the PZN–0.065PT-based composite (see Figs. 3(d)–3(f)) and not valid for the PMN–0.29PT-based composite. Such a difference between the piezoelectric properties of the studied composites is caused by specifics of the piezoelectric anisotropy of the SC components and by smaller elastic compliances $\left|s_{ab}^E\right|$ of the PMN–0.29PT SC in comparison to $\left|s_{ab}^E\right|$ of the PZN–0.065PT SC (see Table 1).

The volume fraction m of SC also influences the piezoelectric anisotropy of the studied composites. Figures 2(a), 3(a), 3(b) and 3(d) suggest that the volume fraction $m = 0.2$ leads to narrow $[\gamma_1; \gamma_2]$ ranges of the validity of conditions (14), and larger volume fractions m become unfavorable to obey conditions (14). In other words, the influence of the SC component on the piezoelectric properties of both the composites at $m > 0.2$ becomes stronger than the influence of the highly anisotropic porous polymer medium at $\rho_p = 100$. As a consequence, $| \zeta_{d1}^* |$ and $| \zeta_{d2}^* |$ from Eq. (9) decrease and become smaller than five at various rotation angles β and γ. It should be also noted that results on the PZN–0.065PT-based composite (see Fig. 3) are more preferable due to its large piezoelectric anisotropy in wider ρ_p and m_p ranges. The large piezoelectric anisotropy at valid conditions (14) enables one to exploit the composite sample as a piezoelectric transducer operating on the longitudinal oscillation mode[7,17] concerned with the piezoelectric coefficient d_{33}^* or electromechanical coupling factor k_{33}^* being proportional to d_{33}^*.

The studied composites are characterized by the validity of conditions

$$(Q_{33}^* / Q_{31}^*)^2 \geq 100 \text{ and } (Q_{33}^* / Q_{32}^*)^2 \geq 100. \qquad (15)$$

Conditions (15) hold simultaneously in specific ranges of the rotation angles β and γ at the aspect ratio $\rho_p = 100$ and porosity $m_p = 0.3$ (Figs. 4 and 5). However, the appropriate volume fraction m of SC in both the composites is relatively small, and we observe a distinct decrease of the (β, γ) region of the validity of conditions (15) when approaching $m = 0.1$ (see Figs. 4(c) and 5(b) on increasing m. This peculiarity is concerned with the influence of the dielectric permittivity $\varepsilon_{pp}^{\sigma}$ of the SC component on the effective piezoelectric coefficients g_{3j}^* and figures of merit $(Q_{3j}^*)^2$ of the composite, see Eqs. (11) and (12). As is known from earlier studies,[7,8] small volume fractions of SC $m \ll 1$ favor the large $|g_{3j}^*|$ values of the 2–2-type composite due to its dielectric permittivity $\varepsilon_{33}^{*\sigma}$ which remains to be relatively small in comparison to $\varepsilon_{pp}^{\sigma}$.

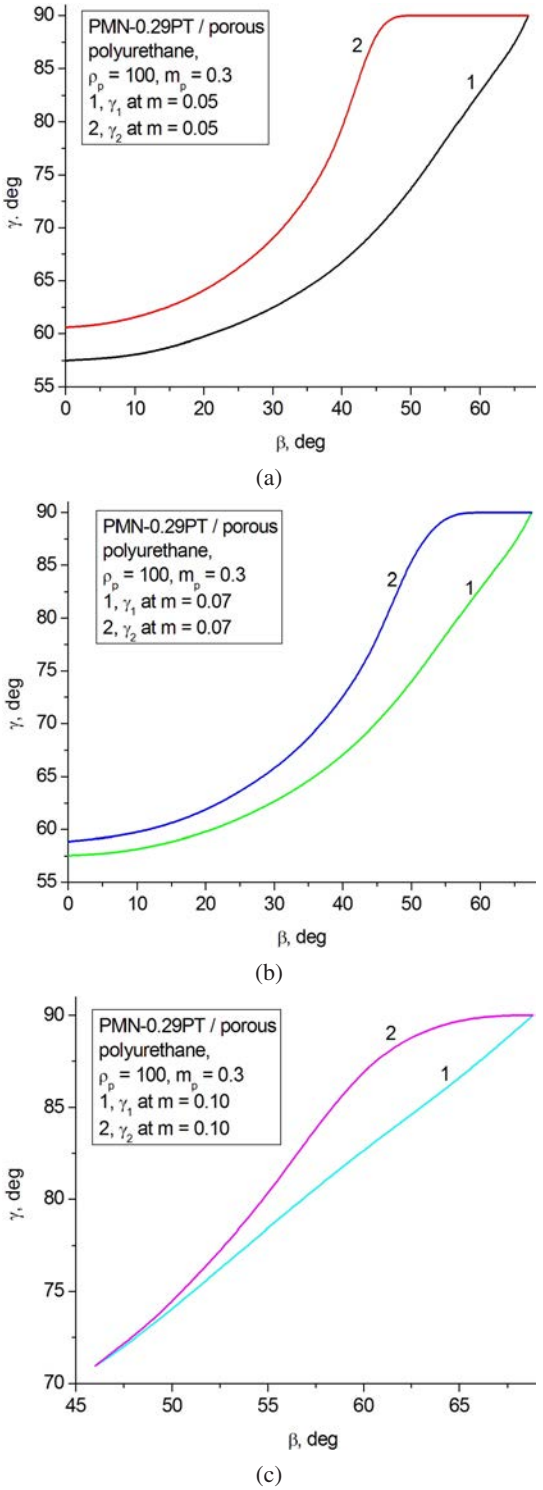

Fig. 4. β–γ diagrams of regions of the large anisotropy of figures of merit $(Q_{3j}^*)^2$ in the 2–2–0 PMN–0.29PT SC/porous polyurethane composite. In the range of $[\gamma_1; \gamma_2]$, conditions (15) hold.

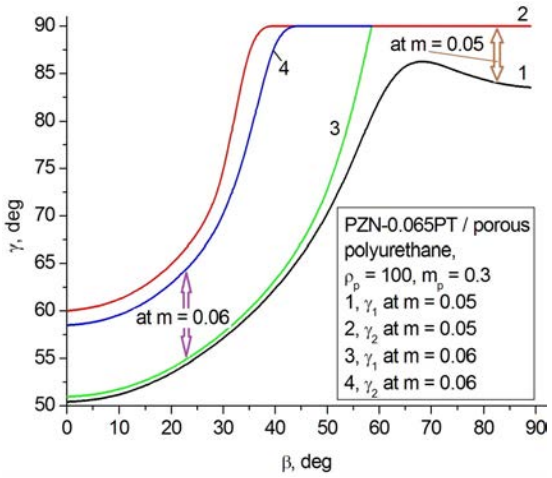

(a)

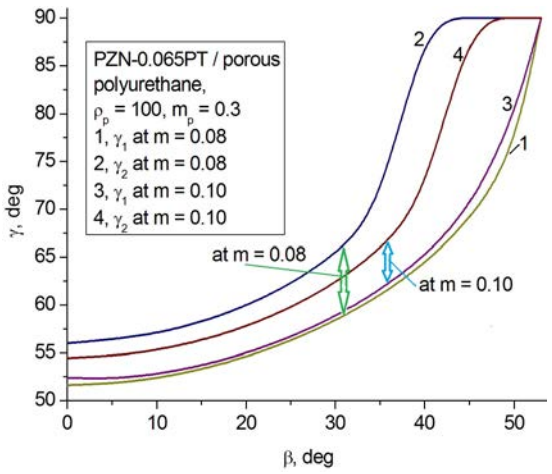

(b)

Fig. 5. β–γ diagrams of regions of the large anisotropy of figures of merit $(Q^*_{3j})^2$ in the 2–2–0 PZN–0.065PT SC/porous polyurethane composite. In the range of $[\gamma_1; \gamma_2]$, conditions (15) hold.

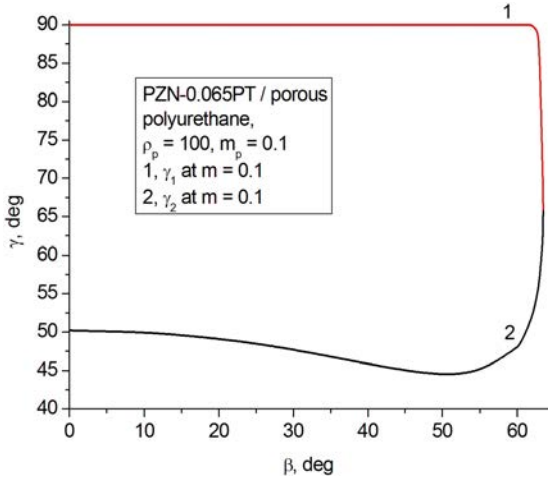

(a)

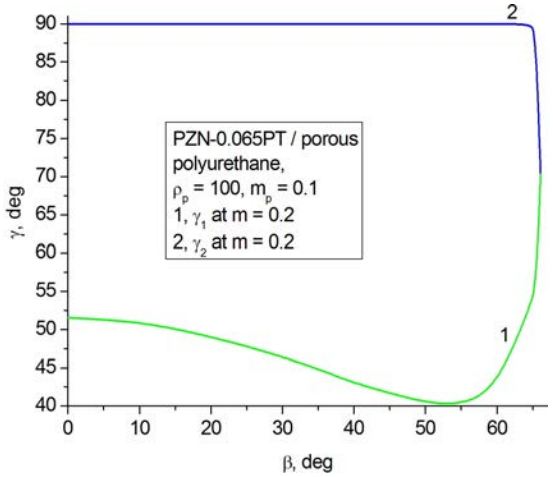

(b)

Fig. 6. β–γ diagrams of the high hydrostatic piezoelectric activity in the 2–2–0 PZN–0.065PT SC/porous polyurethane composite. In the range of $[\gamma_1; \gamma_2]$, condition $d_h^* > 1000$ pC/N holds.

3.2. *Large piezoelectric coefficient d_h^* and advantages of the PZN–0.065PT-based composite*

Among the studied 2–2–0 composites, the PZN–0.065PT-based composite is of keen interest due to its hydrostatic piezoelectric performance. Firstly, even at the small porosity level $m_p = 0.1$, a large hydrostatic piezoelectric coefficient $d_h^* > 1000$ pC/N is achieved (Fig. 6). The (β, γ) region related to the large d_h^* values undergoes minor changes at volume fractions $m = 0.1$–0.2, and these relatively small volume fractions can be regarded as an advantage of the PZN–0.065PT-based composite. We mention for comparison that in the similar PMN–0.29PT-based composite at $\rho_p = 100$, the local max d_h^* increases from 900 pC/N (at porosity $m_p = 0.1$ in the Type II layer) to 1040 pC/N (at $m_p = 0.3$). The smaller values of local max d_h^* are accounted for by the negative piezoelectric coefficient $d_h = -243$ pC/N and smaller piezoelectric coefficients $|d_{3j}|$ of the PMN–0.29PT SC in comparison to its counterpart, PZN–0.065PT SC. For instance, the piezoelectric coefficient d_{33} of PZN–0.065PT is ca. 1.5 times larger than d_{33} of PMN–0.29PT (see Table 1), and the value of $d_h = 144$ pC/N > 0 is achieved in PZN–0.065PT.

Secondly, local max d_h^* values at $m_p = 0.1$ undergo appreciable changes (Table 2) when increasing the aspect ratio ρ_p in the Type II layers from 0.1 to 100. The appropriate volume fraction m_{dh} of SC in the composite is found from the formula max $d_h^* = d_h^*(m_{dh}, \beta, \gamma, \rho_p, m_p)$. From Table 2, a transition from the heavily prolate pore ($\rho_p = 0.1$) to the heavily oblate pore ($\rho_p = 100$) at $m_p = 0.1$ leads to the increase of d_h^* by ca. 3.1 times. The further increase of d_h^* (however less pronounced) is observed on increasing porosity m_p at $\rho_p = 100$, see the bottom part of Table 2. Such changes of d_h^* are accounted for by the influence of the anisotropic elastic properties of porous polymer on the piezoelectric effect and anisotropy of the d^*_{3j}. This anisotropy becomes more appreciable in the presence of the heavily oblate pores, and therefore, contributions from

Table 2. Local maximum values of the hydrostatic piezoelectric coefficient $(d_h^*)_m$ and related volume fractions m_{dh} of SC in the 2–2–0 PZN–0.065PT SC / porous polymer composite.

ρ_p	m_p	$(d_h^*)_m$, pC/N	m_{dh}
0.1	0.1	493	0.402
1	0.1	487	0.400
2	0.1	550	0.384
5	0.1	655	0.362
10	0.1	780	0.321
20	0.1	1130	0.247
50	0.1	1310	0.214
100	0.1	1550	0.150
100	0.2	1800	0.116
100	0.3	1930	0.089

d_{31}^* and d_{32}^* in d_h^* become relatively small. Moreover, the local max d_h^* shifts towards the smaller volume fractions m_{dh} on increasing the aspect ratio ρ_p of the pore (see the 4th column of Table 2).

Thirdly, the graphs in Figs. 7 and 8 suggest that at ρ_p = const and m_p = const, the hydrostatic piezoelectric coefficient d_h^* undergoes appreciable changes on varying the volume fraction m and rotation angle β. The volume fraction m is related to SC being the only piezoelectric component in the composite, and the angle β is concerned with the rotation mode (see the left part of Fig. 1(a)) that influences the longitudinal piezoelectric effect in SC (along the OX_3 axis) to a large extent.

Fourthly, the local max d_h^* is observed in the volume-fraction (m) region where the large anisotropy of the piezoelectric coefficients d_{3j}^* of the composite is achieved. The graphs in Figs. 9(a)–9(c) show that conditions (14) hold undoubtedly. In this context, we emphasize the important role of the β–γ diagrams associated with the large anisotropy of d_{3j}^* (see Fig. 3) in choosing a path to achieve the large d_h^* values in the PZN–0.065PT-based composite. The large local max d_h^* = 1930 pC/N (see Figs. 7 and 8) is achieved at the longitudinal piezoelectric coefficient $d_{33}^* \approx 2290$ pC/N (see Fig. 9(c)), i.e., we obtain $d_h^*/d_{33}^* \approx 0.84$. The relatively small volume fraction of SC m_{dh} = 0.089 means that the Type II layers with the heavily oblate pores strongly influence the piezoelectric coefficients d_{3j}^* and suppress the transversal piezoelectric effect (at j = 1 and 2) to a large extent. In addition, the large elastic compliance $s_{33}^{(0-3)}$ of the Type II layer at ρ_p = 100 promotes the intensive increase of the piezoelectric coefficient d_{33}^* of the composite at volume fractions $m \ll 1$, see Figs. 9(a)–9(c).

3.3. *Some comparisons and remarks*

The graph in Fig. 9(d) shows the volume-fraction (m) dependence of the longitudinal figure of merit $(Q_{33}^*)^2$ that has a maximum at $m \ll 1$ by analogy with the piezoelectric

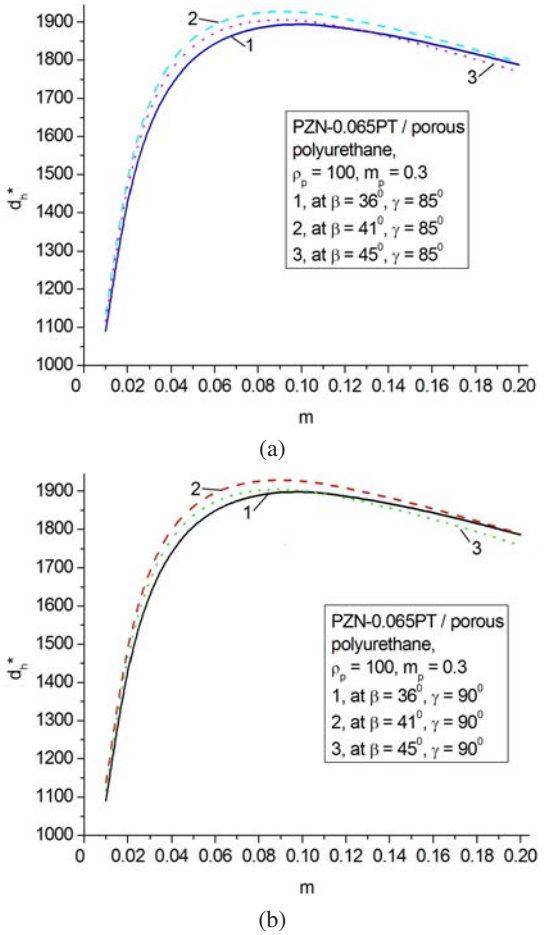

Fig. 7. Volume-fraction (m) dependences of the hydrostatic piezoelectric coefficient d_h^* (in pC/N) in the 2–2–0 PZN–0.065PT SC/ porous polyurethane composite.

coefficient g_{33}^*. This non-monotonic behavior is caused by the strong influence of the dielectric properties of the composite on the piezoelectric coefficient g_{33}^* and, therefore, on $(Q_{33}^*)^2$ associated with g_{33}^* in accordance with Eq. (11). Comparing curves 1–3 in Fig. 9(d), we note that an appreciable difference between the $(Q_{33}^*)^2$ values related to different porosity levels (m_p = 0.1–0.3) is concerned with the aforementioned influence of the dielectric properties at $m \ll 1$. Now we should consider the influence of porosity m_p on the dielectric properties of the composite. Despite the decreasing character of the volume-fraction dependence of $(Q_{33}^*)^2$ in the vicinity of m_{dh} = 0.089, we note the large level of the $(Q_{33}^*)^2$ values (see Fig. 9(d)) in comparison to the typical $(Q_{33})^2$ values of domain-engineered relaxor-ferroelectric SCs. For instance, taking experimental data from Table 1 into account, we evaluate the following figure of merit of the SC component at $\beta = \gamma = 0°$ (i.e., in the main crystallographic axes): $(Q_{33})^2 = 49.8 \cdot 10^{-12}$ Pa^{-1} for PZN–0.065PT or $(Q_{33})^2 = 29.7 \cdot 10^{-12}$ Pa^{-1} for PMN–0.29PT.

The large anisotropy of the piezoelectric coefficients d_{3j}^* promotes a large hydrostatic piezoelectric coefficient d_h^*,

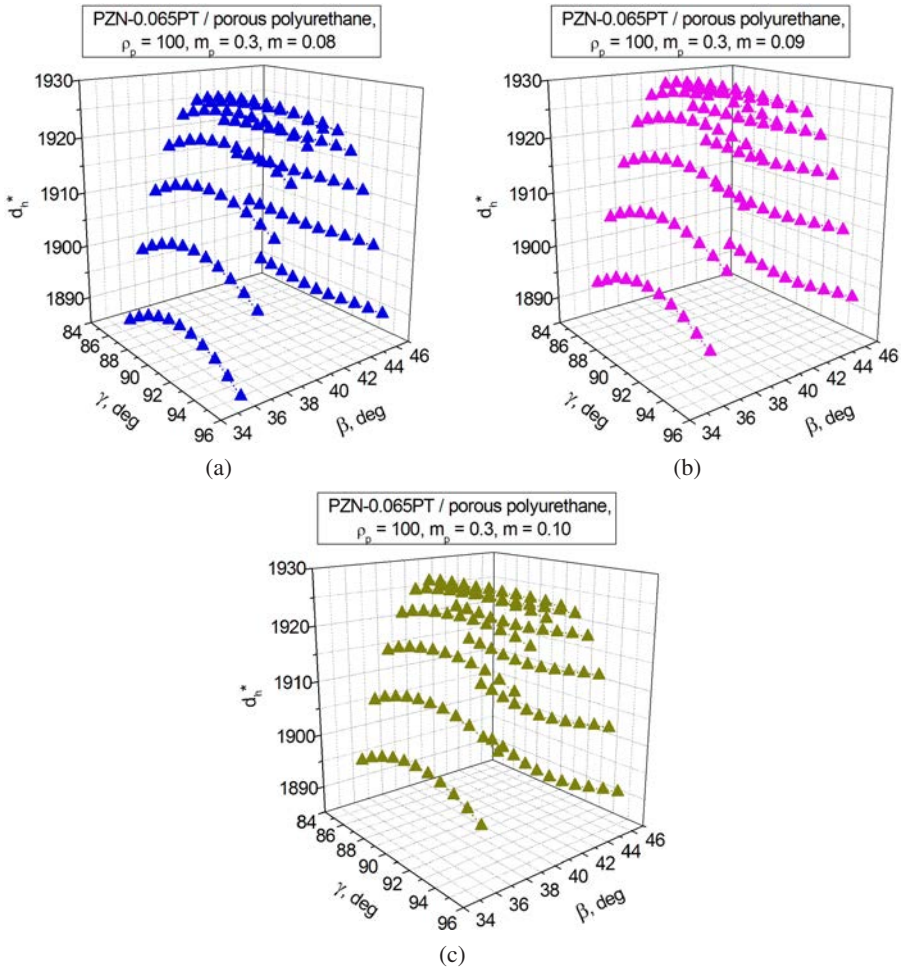

Fig. 8. Orientation (β, γ) dependences of the hydrostatic piezoelectric coefficient d_h^* (in pC/N) in the 2–2–0 PZN–0.065PT SC/porous polyurethane composite.

and its positive value in the PMN–0.29PT-based composite becomes approximately four times larger than $| d_h |$ of the SC component (i.e., d_h^* at $m = 1$ and $\beta = \gamma = 0°$). Such a change of the sign of d_h^* and variations of d_h^* from negative values to $d_h^* \approx 1000$ pC/N were not discussed earlier in detail and become a serious argument that supports the active role of the orientation and porosity effects in the PMN–0.29PT-based composite. In comparison to this, the PZN–0.065PT-based composite demonstrates variations of $d_h^* > 0$ in a wide range, so that the local max d_h^* shown in Figs. 7 and 8 is ca. 13 times larger than d_h of the SC component. Such a wide range is due to the two aforementioned effects acting together. It should be added that 2–2 [011]-poled domain-engineered PMN–xPT SC/polymer composites[1] are characterized by the hydrostatic piezoelectric coefficient d_h^* = 170–570 pC/N, and values of d_h = 70–180 pC/N are known from experiments[1] on the SC components.

The large ratio of $d_h^*/{d_{33}}^* \approx 0.84$ (see Sec. 3.2) can be compared to the ratio of $d_h^*/{d_{33}}^* \approx 0.80$–$0.93$ that is achieved in 2–0–2–0 porous PZT-type ceramic/porous polymer composites[21] with two systems of closed air pores. These 2–0–2–0 composites are characterized by the hydrostatic piezoelectric coefficient[21] $d_h^* \approx$ 300–500 pC/N that is relatively large in comparison to the similar parameter of the poled ceramic and relatively small in comparison to the local max d_h^* values of the 2–2–0 composites described in the present paper (see Sec. 3.2). Undoubtedly, such a level of the d_h^* values in the 2–0–2–0 composites is inextricably linked to a smaller piezoelectric activity of their ceramic component[21] in comparison to the domain-engineered SC component from the present study.

The orientation effect studied in the 2–2–0 composites is stronger than that observed in oriented 2–2 and 3–3 ceramic/polymer composites.[22,23] This can be concerned with ¥*mm* symmetry and electromechanical properties of the poled ferroelectric ceramic.[17] Its piezoelectric coefficients obey conditions $d_{31} = d_{32} < 0$ and $d_{33} > 0$ for numerous PZT-type compositions, and the piezoelectric anisotropy is small (as a rule, $| d_{33}/d_{31} | < 3$).[7,8,24]

A formation of piezoelectric textures leads to an increase of piezoelectric coefficients, figures of merit and related parameters of materials. A longitudinal figure of merit of

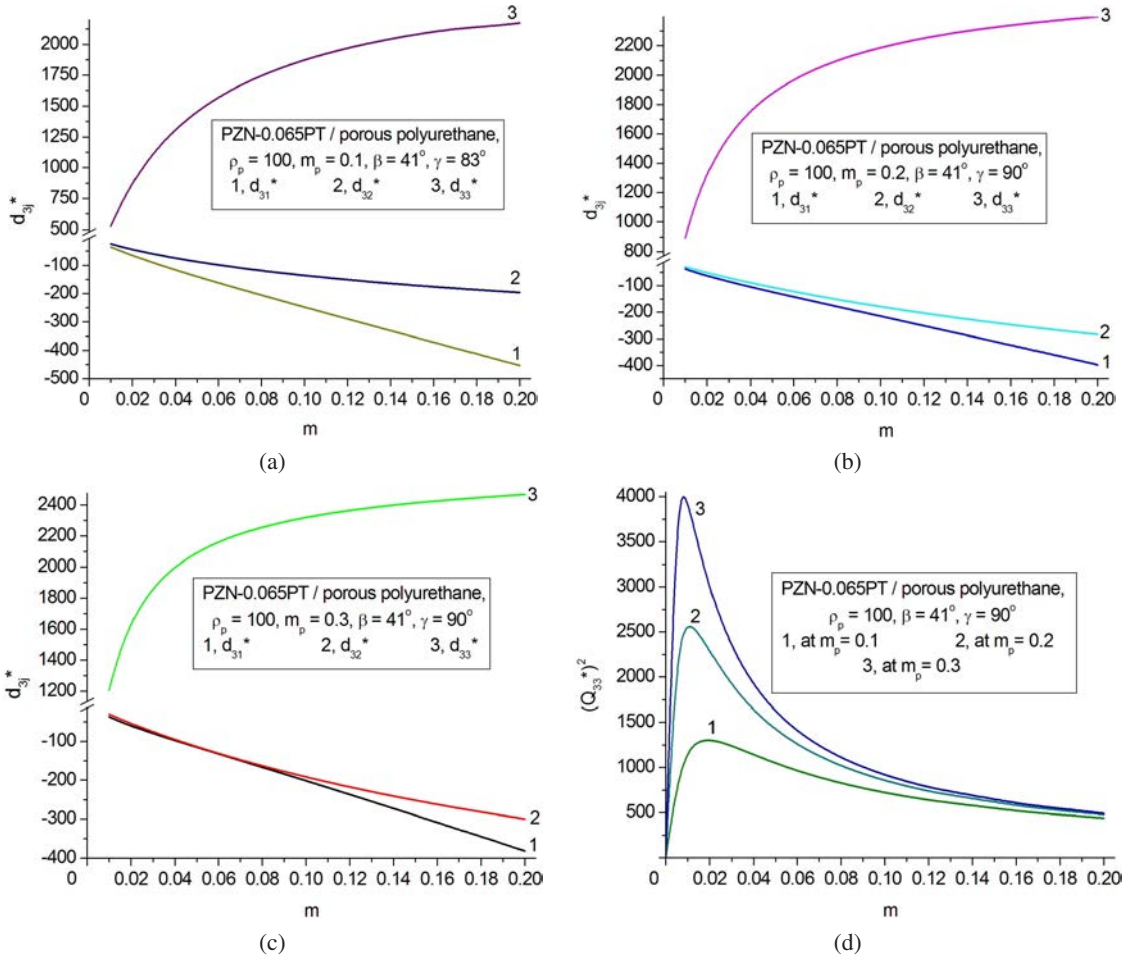

Fig. 9. Volume fraction (m) behavior of piezoelectric coefficients d_{3j}^* (a–c, in pC/N) and figure of merit $(Q_{3j}^*)^2$ (d, in 10^{-12} Pa^{-1}) in the 2–2–0 PZN–0.065PT SC/porous polyurethane composite near the local max d_h^* shown in Figs. 7 and 8.

a textured $Pb(Mg_{1/3}Nb_{2/3})O_3 - PbZrO_3 - PbTiO_3$ ceramic[25] with a high piezoelectric performance is $(Q_{33})^2 = 59.18 \cdot 10^{-12}$ Pa^{-1}, and this value is large in comparison to $(Q_{33})^2$ of conventional poled ceramics,[7,8] however, an order-of-magnitude is smaller than that of $(Q_{33}{}^*)^2$ of the 2–2–0 composite at volume fractions $m \approx 0.1$–0.2 (see Fig. 9(d)). The noticeable increase in $(Q_{33}{}^*)^2$ of the studied 2–2–0 composites in comparison to the $(Q_{33})^2$ value of the textured ceramic[25] is caused by the domain-engineered SC component and orientation and porosity effects acting together.

4. Conclusions

Our present paper has been devoted to two effects that act together in the advanced piezo-active 2–2-type composite based on the domain-engineered [011]-poled SC (see Fig. 1(a)). The first effect is concerned with the strong dependence of the effective piezoelectric properties and related parameters of the composite on the orientation of the main crystallographic axes in SC (Type I layer). This orientation is described in terms of the rotation angles β and γ. The second effect is associated with the influence of porous polymer (microgeometry and porosity) in the Type II layers on the piezoelectric performance and related parameters of the composite. Conditions (14) for the large piezoelectric anisotropy hold for both the studied composites in specific ranges of orientation angles and porosity. The diagrams have been built for the first time to show the (β, γ) regions, where the large anisotropy of the piezoelectric coefficients d_{3j}^* [or energy-harvesting figures of merit $(Q_{3j}^*)^2$] is achieved (see Figs. 2–5), and where the condition for the hydrostatic piezoelectric coefficient $d_h{}^* > 1000$ pC/N holds (see Fig. 6). The large local max $d_h{}^* = 1930$ pC/N is achieved in the 2–2–0 PZN–0.065PT-based composite (see Figs. 7 and 8) at the longitudinal piezoelectric coefficient $d_{33}{}^* \approx 2290$ pC/N and figure of merit $(Q_{33}{}^*)^2 \approx 1 \cdot 10^{-9}$ Pa^{-1} (see Fig. 9). The large piezoelectric coefficients, anisotropy factors and figures of merits, which are achieved in the studied 2–2-type composites, are to be of value in sensing, energy-harvesting and hydroacoustic applications.

Acknowledgments

We are grateful to Prof. Dr. I. A. Parinov and Prof. Dr. A. E. Panich (Southern Federal University, Russia), Prof. Dr. C. R. Bowen (University of Bath, UK), and Prof. Dr. P. Bisegna (University of Rome Tor Vergata, Italy) for their interest in high-performance piezoelectric materials. We thank Prof. Dr. C. R. Bowen for his careful reading of the manuscript in the final stage. Research was supported by the Southern Federal University (research topic "Development and Materials-Science Substantiation of the Creation of Materials and Products Based on Piezoelectric Ceramics Using Additive Technologies", stage 2022, contract No. 176/22-D, July 11th, 2022).

References

[1]L. Li, S. Zhang, Z. Xu, X. Geng, F. Wen, J. Luo and T. R. Shrout, Hydrostatic piezoelectric properties of [011] poled $Pb(Mg_{1/3}Nb_{2/3})O_3$-$PbTiO_3$ single crystals and 2-2 lamellar composites, *Appl. Phys. Lett.* **104**, 032909 (2014).

[2]Q. Yue, D. Liu, J. Deng, X. Zhao, D. Lin, W. Di, X. Li, W. Wang, X. Wang and H. Luo, Design and fabrication of relaxor-ferroelectric single crystal PIN–PMN–PT/epoxy 2–2 composite based array transducer, *Sens. Actuat. A. Phys.* **234**, 34 (2015).

[3]S. Hou, X. Yang, C. Fei, X. Sun, Q. Chen, P. Lin, D. Li, Y. Yang and Q. Zhou, Fabrication of PMN-PT/epoxy 2–2 composite ultrasonic transducers and analysis based on equivalent circuit model, *J. Electron. Mater*. **47**, 6842 (2018).

[4]J. Wang, M. Chen, X. Zhao, F. Wang, Y. Tang, D. Lin and H. Luo, Fabrication and high acoustic performance of high frequency needle ultrasound transducer with PMN-PT/Epoxy 1-3 piezoelectric composite prepared by dice and fill method, *Sens. Actuat. A. Phys.* **318**, 112528 (2021).

[5]J. Ma, D. Huo, X. Qi, K, Zhu, B. Shen, Y. Liu and R. Zhang, Enhanced electromechanical properties in $Pb(Mg_1/3Nb_2/3)O_3$–$PbTiO_3$ based 1–3 piezoelectric composites using the alternating current poling method, *Mater. Sci. Eng. B* **284**, 115890 (2022).

[6]E. Sun and W. Cao, Relaxor-based ferroelectric single crystals: Growth, domain engineering, characterization and applications, *Prog. Mater. Sci.* **65**, 124 (2014).

[7]C. R. Bowen, V. Yu. Topolov and H. A. Kim, *Modern Piezoelectric Energy-Harvesting Materials* (Springer International Publishing Switzerland, Cham, 2016).

[8]J. I. Roscow, V. Yu. Topolov, C. R. Bowen and H. Khanbareh, *Innovative Piezo-Active Composites and Their Structure – Property Relationships* (World Scientific, Singapore, 2022).

[9]N. E. Cabrera-Munoz, P. Eliahoo, R. Wodnicki, H. Jung, C. T. Chiu, J. A. Williams, H. H. Kim, Q. Zhou and K. K, Shung, Forward-looking 30-MHz phased-array transducer for peripheral intravascular imaging, *Sens. Actuat. A. Phys.* **280**, 145 (2018).

[10]Z. Zeng, L. Gai, A. Petitpas, Y. Li, H. Luo, D. Wang and X. Zhao, A flexible, sandwich structure piezoelectric energy harvester using PIN-PMN-PT/epoxy 2-2 composite flake for wearable application, *Sens. Actuat. A. Phys.* **265**, 62 (2017).

[11]Y. Chen, K.-H. Lam, D. Zhou, Q. Yue, Y. Yu, J. Wu, W. Qiu, L. Sun, C. Zhang, H. Luo, H. L. W. Chan and J. Dai, High performance relaxor-based ferroelectric single crystals for ultrasonic transducer applications, *Sensors* **14**, 13730 (2014).

[12]V. Yu. Topolov, C. R. Bowen, A. V. Krivoruchko and A. N. Isaeva, Orientation effects and figures of merit in advanced 2–2-type composites based on [011]-poled domain-engineered single crystals, *CrystEngComm* **24**, 1177 (2022).

[13]R. Zhang, B. Jiang and W. Cao, Elastic, piezoelectric, and dielectric properties of multidomain $0.67Pb(Mg_{1/3}Nb_{2/3})O_3 - 0.33PbTiO_3$ single crystals. *J. Appl. Phys.* **90**, 3471 (2001).

[14]F. Wang, L. Luo and D. Zhou, Complete set of elastic, dielectric, and piezoelectric constants of orthorhombic $0.71Pb(Mg_{1/3}Nb_{2/3})O_3 - 0.29PbTiO_3$ single crystal, *Appl. Phys. Lett.* **90**, 212903 (2007).

[15]S. Zhang and L. C. Lim, Property matrices of [011]-poled rhombohedral $Pb(Zn_{1/3}Nb_{2/3})O_3$–(4.5-7)%$PbTiO_3$ single crystals, *AIP Adv.* **8**, 115010 (2018).

[16]R. E. Newnham, D. P. Skinner and L. E. Cross, Connectivity and piezoelectric-pyroelectric composites, *Mater. Res. Bull*. **13**, 525 (1978).

[17]T. Ikeda, *Fundamentals of Piezoelectricity* (Oxford University Press, Oxford, New York, Toronto, 1990).

[18]M. L. Dunn and M. Taya, Electromechanical properties of porous piezoelectric ceramics, *J. Am. Ceram. Soc.* **76**, 1697 (1993).

[19]J. H. Huang and W.-S. Kuo, Micromechanics determination of the effective properties of piezoelectric composites containing spatially oriented short fibers, *Acta Mater*. **44**, 4889 (1996).

[20]B. Noheda, Structure and high-piezoelectricity in lead oxide solid solutions, *Curr. Opin. Solid State Mater. Sci*. **6**, 27 (2002).

[21]A.A. Nesterov, V. Yu. Topolov, M. I. Tolstunov and A. N. Isaeva, Longitudinal piezoelectric effect and hydrostatic response in novel laminar composites based on ferroelectric ceramics, *Ceram. Int*. **45**, 22241 (2019).

[22]E. K. Akdogan, M. Allahverdi and A. Safari, Piezoelectric composites for sensor and actuator applications, *IEEE Trans. Ultrason. Ferroelectr. Freq. Control* **52**, 746 (2005).

[23]A. Safari, M. Allahverdi and E. K. Akdogan, Solid freeform fabrication of piezoelectric sensors and actuators, *J. Mater. Sci*. **41**, 177 (2006).

[24]Y. Xu, *Ferroelectric Materials and Their Applications* (North-Holland, Amsterdam, 1991).

[25]Y. Yan, K.-H. Cho, D. Maurya, A. Kumar, S. Kalinin, A. Khachaturyan and S. Priya, Giant energy density in [001]-textured $Pb(Mg_{1/3}Nb_{2/3})O_3$ – $PbZrO_3$ – $PbTiO_3$ piezoelectric ceramics, *Appl. Phys. Lett*. **102**, 042903 (2013).